

The Fastest Travel Together: Chemical Tagging of the Fastest Stars in Gaia DR2 to the Stellar Halo

Keith Hawkins^{1*} and Rosemary F. G. Wyse^{2,3}

¹*Department of Astronomy, The University of Texas at Austin, 2515 Speedway Boulevard, Austin, TX 78712, USA*

²*Physics and Astronomy Department, Johns Hopkins University, 3400 North Charles Street, Baltimore, MD 21218, USA*

³*Leverhulme Trust Visiting Professor, University of Edinburgh, UK*

Accepted 2018 August 13. Received 2018 August 12; in original form 2018 June 14

ABSTRACT

The fastest moving stars provide insight into several fundamental properties of the Galaxy, including the escape velocity as a function of Galactocentric radius, the total mass, and the nature and frequency of stellar encounters with the central Supermassive Black Hole. The recent second data release of *Gaia* has allowed the identification of new samples of stars with extreme velocities. Discrimination among the possible origins of these stars is facilitated by chemical abundance information. We here report the results from our high-resolution spectroscopic followup, using the Apache Point Observatory, of five late-type ‘hypervelocity’ star candidates from [Marchetti et al. \(2018\)](#), characterised by derived total Galactic rest-frame velocities between 500–600 km s^{−1} and estimated, by those authors, to have a probability larger than 50% to be unbound from the Milky Way. Our new results confirm the *Gaia* DR2 radial velocities to within 1 km s^{−1}. We derived stellar atmospheric parameters and chemical abundances for several species including α -elements (Mg, Ti, Si, Ca), Fe-peak elements (Fe, Ni, Co, Cr, Mn), neutron-capture elements (Sr, Y, Zr, Ba, La, Nd, Eu) and odd-Z elements (Na, Al, K, V, Cu, Sc). We find that all stars observed are metal-poor giants with $-2 \leq [\text{Fe}/\text{H}] \leq -1$ dex and are chemically indistinguishable from typical halo stars. Our results are supported by the chemical properties of four additional stars with extreme space motions which were observed by existing spectroscopic surveys. We conclude that these stars are simply the high-velocity tail of the stellar halo and effectively rule out more exotic origins such as from the Galactic centre or the Large Magellanic Cloud.

Key words: Stars: kinematics and dynamics, Stars: Population II, Stars: abundances

1 INTRODUCTION

The fastest moving stars observed within the Galaxy provide insight into several fundamental properties of the Galaxy, including the escape velocity (potential well depth) as a function of Galactocentric radius and the total mass (e.g. [Piffl et al. 2014](#); [Rossi et al. 2017](#)), and the nature and frequency of stellar encounters with the central Supermassive Black Hole (e.g. [Rossi et al. 2017](#)). Despite their importance, the nature of these rare objects and their ejection mechanisms remain poorly understood (reviewed in [Brown 2015](#)).

The existence of ‘hypervelocity’ stars (HVSs)¹, moving at speeds in excess of 1000 km s^{−1}, was first predicted by

[Hills \(1988\)](#), being produced as a result of triple-body encounters between binary stellar systems and the putative supermassive black hole (SMBH) at the Galactic Centre. They remained a theoretical fascination until the early 2000s when [Brown et al. \(2005\)](#) serendipitously discovered a 3 M_⊙ B-type star at a distance of 100 kpc and with a Galactic rest frame radial velocity above 700 km s^{−1}, indicating that it was unbound to the Milky Way. The advent of several large spectroscopic and astrometric surveys has greatly increased the potential of finding and characterising these interesting rare stars has led to significant growth in this subfield.

Over the last decade, there has been significant interest in understanding whether other production mechanism could be responsible for the origin of HVSs. Several mechanisms other than the ‘Hills’ mechanism have been proposed. These include the ejection of a binary companion when the primary star undergoes a supernova (e.g. [Blaauw 1961](#)), tidal debris from dwarf galaxies ([Abadi et al. 2009](#)), dynam-

* E-mail: keithhawkins@utexas.edu

¹ In this study we define hypervelocity stars as those whose velocity is estimated to be larger than the escape speed and thus unbound. This definition is agnostic to the production mechanism.

ical ejection from dense stellar clusters (Poveda et al. 1967; Bromley et al. 2009), acceleration from the jets of Active Galactic Nuclei (e.g. Silk et al. 2012; Wang & Loeb 2017), among others. The various different production mechanisms will have different observational signatures in the spatial, kinematic, and chemical distributions. However, there are only ~ 20 confirmed HVSs.

With the recent second data release of data from the *Gaia* astrometric mission (*Gaia* DR2), there has been a concerted effort to search for the fastest moving stars in the Galaxy, motivated by a range of scientific questions. For example, Shen et al. (2018) report the discovery of three white dwarfs with derived space motions over 1000 km s^{-1} , plausibly survivors of double-detonation events. Boubert et al. (2018) examine the status of hypervelocity stars, with an emphasis on late-type stars. Even though many candidates analysed by Boubert et al. (2018) are not likely to be actually unbound stars, the new data have enabled the identification of many new candidate extreme-velocity stars at a higher level of significance. Marchetti et al. (2018) and Hattori et al. (2018) both undertake a systematic search for the fastest moving stars in *Gaia* DR2, using the total velocity vector of a star, or just its Galactic rest frame tangential motion, respectively. The *Gaia* data also allow the orbits of extreme-velocity stars to be derived, once a model for the Galactic potential is adopted (e.g. Brown et al. 2018). These recent studies make it clear that there has been a recent rapid increase in the number of candidate late-type extreme velocity stars identified and characterising their orbital *and* chemical properties will be critical to understand their origins.

The discovery of new late-type candidate extreme-velocity stars from *Gaia* DR2 warrants spectroscopic followup. The purpose of this work is to communicate the results from our high-resolution spectroscopic followup of five late-type candidates from the sample of extreme-velocity stars identified by Marchetti et al. (2018). The aim of this paper is two fold: (i) confirm (or not) the radial velocity (RV) reported by *Gaia* (many have very high RVs, which the *Gaia* team caution against using *Gaia* Collaboration et al. 2018), and (2) provide detailed characterization of these stars in terms of both stellar atmospheric parameters and chemistry, in order to better understand their origins.

With these aims in mind, this paper is arranged as follows: in section 2.1, we review the selection criteria of HVS candidates using *Gaia* DR2, which were defined in Marchetti et al. (2018). We then outline the high-resolution spectroscopic followup that we completed (section 2.2) and our search to find if any of the HVS candidates have serendipitously been observed by any of several large spectroscopic surveys with publicly available data (section 2.3). In section 3 we describe the methods that were used to derive the RV, stellar parameters and chemical abundances for 22 species. The results confirming the RVs and determining the stellar parameters and chemical abundances in 4 elemental families (α , odd-Z, Fe-peak, neutron capture) are described in section 4. These results are then placed into the context of how HVSs may have formed in section 4.6. Finally, we summarize our results in section 5.

2 DATA

2.1 Selecting Extreme Velocity Stars from *Gaia* DR2

There are various possible criteria and selection techniques that may be used to identify candidate extreme-velocity stars. Prior to the precise astrometric data from *Gaia*, a high value of the Galactic rest-frame radial velocity was used (e.g. Brown et al. 2005; Smith et al. 2007; Piffi et al. 2014; Hawkins et al. 2015). The use of high proper-motion to identify ‘high-velocity’ (relative to the Sun) halo stars has a long history (e.g. Eggen et al. 1962; Carney et al. 1994). The addition of parallax information allows the adoption of high tangential velocity in the Galactic rest frame as the criterion, as utilised by Hattori et al. (2018). The addition of radial velocities allows the adoption of high 3-dimensional space motion, as utilised by Marchetti et al. (2018). We here select stars from the extreme-velocity sample defined by Marchetti et al. (2018) and we review their procedure next.

Marchetti et al. (2018) first divided the over-seven million stars in the *Gaia* DR2 catalogue with both radial velocity and 5-parameter astrometric solution into a high-quality subsample (with fractional parallax uncertainties below 20%, (6376803 stars) and a low-quality subsample (806459 stars). They derived distances for the high-quality subsample by simple inversion of the parallax, while for the low-quality subsample distances were inferred from the parallax using the procedure of Astraatmadja & Bailer-Jones (2016). The 3-d space-velocity vectors for stars in both subsamples were derived using the full covariance matrix in proper-motion space. These authors then implemented some quality-control cuts (see their section 4), to ensure, for example, that the astrometric model was a good fit to the data obtained from *Gaia*. They then applied a minimum velocity threshold such that the absolute value of the 3-d Galactic rest-frame velocity be larger than 450 km s^{-1} . This resulted in a sample of 165 high-velocity stars, most of which lie on the red-giant locus in the HR Diagram and are located a few kpc from the Sun. Marchetti et al. (2018) then adopted a model Galactic potential (see their section 4.1 for details) and identified 28 extreme-velocity stars that they estimated to have a greater than 50% probability of being on unbound orbits. These authors further used the derived orbit to infer whether a given star could have originated in the Galactic Centre or from a location within the disc. We have drawn our sample for high-resolution spectroscopic followup from this final set of stars (their Table 1).

However, it is critical to keep in mind that there are other valid procedures for selecting HVS candidates. For example, Hattori et al. (2018) search for HVS candidates not from full 3-d space motions as in Marchetti et al. (2018) but rather using the Galactic rest frame tangential velocity corrected for the Solar reflex motion. They found a total of 30 extreme-velocity stars. Another way is to use the Galactic rest-frame radial velocity to select high-velocity stars (e.g. Hawkins et al. 2015). Each of these methods is valid and should be combined to find the best candidates for unbound HVSs.

Table 1. Observational Properties of Candidate Extreme-velocity Stars and Radial Velocity Standards

Star	RA (deg)	DEC (deg)	G (mag)	RV_{Gaia} (km s ⁻¹)	RV_{APO} (km s ⁻¹)	V_{tot} (km s ⁻¹)	P_{MW}	P_{ub}	SNR	t_{obs} (s)
1508756353921427328	210.2049	45.86615	12.63	128.22±1.3	122.68±0.30	515	0.99	0.58	44	1800
1364548016594914560	268.7792	50.57305	11.93	110.36±44	109.50±0.20	531	1.00	0.74	46	1800
4593398670455374592	274.8965	33.81894	12.24	-312.96±1.15	-314.60±0.23	545	0.55	0.58	42	1800
4248140165233284352	299.6680	04.51105	13.21	-358.10±2.28	-358.29±0.17	567	0.50	0.56	42	1800
2233912206910720000	299.2838	55.49696	12.97	-343.93±1.71	-344.19±0.50	540	0.42	0.76 ^a	34	1800
RV standards										
HD 122563	210.6318	9.68579	5.85	-26.16±0.16	-26.57±0.64	210	60
HD 84937	147.2354	13.7409	8.19	-15.69±0.42	-15.50±0.50	150	600

NOTE: The identifier of each star is given in column 1, with coordinates in columns 2 and 3. The G -band magnitude is tabulated in column 4. The radial velocity measured by *Gaia* and by our high-resolution spectra are in column 5 and column 6, respectively, with the 3-d speed in column 7. The probabilities of the star originating in the Milky Way disc (P_{MW}) and of being unbound to the Galaxy (P_{ub}) are taken from Marchetti et al. (2018) and given in columns 8 and 9 respectively. ^a Hattori et al. (2018) derive a probability of 0.84 for this star being unbound from the potential they adopt. Columns 10 and 11 give, respectively, the signal-to-noise ratio measured in the $\lambda \sim 5300\text{--}5400$ Å range and the exposure time in seconds required to obtain the signal-to-noise ratio.

2.2 Observational Follow-up and Reduction

We selected five candidate extreme-velocity stars, accessible from Apache Point Observatory (APO) in May 2018, from the sample of Marchetti et al. (2018). Of these five, three have derived orbits consistent with an origin in the Galactic centre while the other two do not. We obtained high-resolution ($R = \lambda/\Delta\lambda \sim 31500$) optical spectra for each of these stars, using the ARC Echelle Spectrograph (ARCES) on the APO 3.5m telescope, during the nights of 2-May-2018 and 7-May-2018. The spectra have wavelength coverage 3800–9200 Å over ~ 107 echelle orders. We also obtained spectra for two bright radial-velocity standard stars (HD 84937 and HD 122563). Standard calibration images (biases, flat fields, and ThAr arc lamps) were taken. The spectra were reduced using the standard methods of: bias subtraction, extraction, flat field division, scattered light subtraction, and stacking using the echelle package of IRAF². An initial continuum normalization for order stitching was done assuming a 5th-order spline function. RVs were measured using cross-correlation with an Arcturus spectral template. When multiple spectra of the same object were taken, the individual spectra were co-added to obtain a higher signal-to-noise ratio (SNR).

The final high-resolution spectra of the five extreme-velocity targets have a typical SNR ~ 40 pixel⁻¹. The basic observational properties of these stars (plus the standard stars) are given in Table 1, including coordinates, *Gaia* G band magnitude, radial velocity as measured in both *Gaia* and this study, and the typical SNR. Figure 1 shows the final reduced, extracted, wavelength calibrated, and RV corrected spectra in the Mg-triplet region (5135–5215 Å). These spectra were used to carry out our scientific aims, namely to confirm (or not) the *Gaia* radial velocities, characterise the atmospheric parameters and in particular the chemical properties of these rare stars and hence investigate how they

might be associated, via ‘chemical tagging’, with known populations within the Milky Way or LMC.

2.3 Large Spectroscopic Surveys : Data From APOGEE, LAMOST, and RAVE

We cross matched the extreme-velocity candidate sample from Table 1 of Marchetti et al. (2018) with the public databases of four large spectroscopic surveys, namely APOGEE DR14 (Majewski et al. 2017, Holtzman et al., in prep.), LAMOST DR3 (Luo et al. 2015; Xiang et al. 2017), RAVE DR5 (Kunder et al. 2017) and GALAH DR2 (Buder et al. 2018). We found 1 star (*Gaia* DR2 1268023196461923712) in common with APOGEE, 3 stars (*Gaia* DR2 6639557580310606976, *Gaia* DR2 5212817273334550016, and *Gaia* DR2 4916199478888664320) in common with the RAVE survey, 1 star (*Gaia* DR2 1268023196461923712) in common with the LAMOST survey and no stars in common with the GALAH survey. The basic observational data for these stars are given in Table 2.

3 HIGH-RESOLUTION SPECTROSCOPIC ANALYSIS

Spectroscopic analysis was done using the Brussels Automatic Code for Characterizing High accuracy Spectra (BACCHUS, Masseron et al. 2016). The current released version makes use of the MARCS model atmosphere grid (Gustafsson et al. 2008), and the radiative transfer code TURBOSPECTRUM (Alvarez & Plez 1998; Plez 2012) to generate synthetic spectra for comparison with the observations. Atomic lines are sourced from the fifth version of the *Gaia*-ESO linelist (Heiter et al., in preparation). In addition to the atomic lines, linelists for molecular species are also used in the calculation of synthetic spectra. The molecular species included are CH (Masseron et al. 2014), and CN, NH, OH, MgH and C₂(T. Masseron, private communication); the lines of SiH molecules are adopted from the Kurucz linelists

² Distributed by NAO, operated by AURA under cooperative agreement with the NSF.

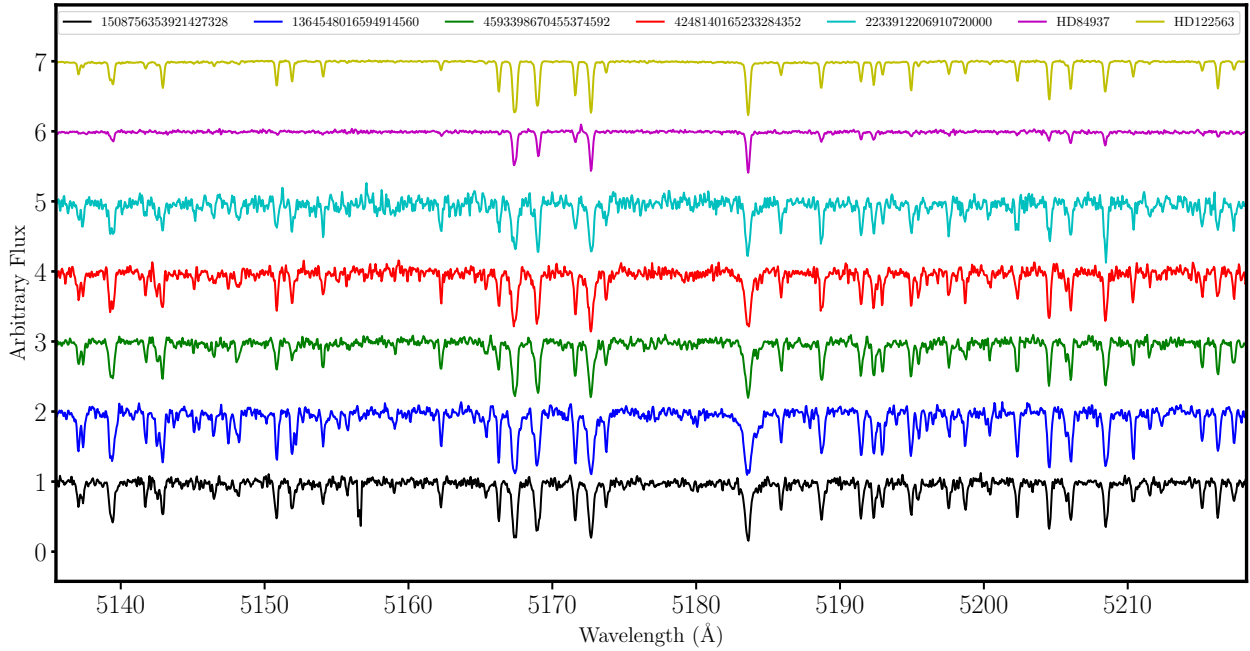


Figure 1. Illustrates the observed spectra in the Mg triplet region (5135–5215 Å) of the two bright standard stars (HD 122563, HD 84937) and the five candidate HVs observed in this work, namely *Gaia* DR2 1508756353921427328, *Gaia* DR2 1364548016594914560, *Gaia* DR2 4593398670455374592, *Gaia* DR2 4248140165233284352 and *Gaia* DR2 2233912206910720000 from top to bottom, respectively.

Table 2. Observational Properties of Extreme-velocity Star Candidates from other surveys

Star	RA (deg)	DEC (deg)	<i>G</i> (mag)	RV_{Gaia} (km s ⁻¹)	RV_{survey} (km s ⁻¹)	V_{tot} (km s ⁻¹)	P_{MW}	P_{ub}	SNR	Survey
1268023196461923712	225.7835	26.24632	13.00	-276.84±1.64	-275.49±0.03 ^a	551	0.49	0.62	119	A, L
6639557580310606976	287.9278	-57.80599	12.26	-257.08±1.19	-255.59±0.75	581	0.38	0.62	63	R
5212817273334550016	107.1991	-76.21933	10.89	159.87±0.29	157.97±0.44	568	0.35	0.79	81	R
4916199478888664320	23.38253	-51.92318	12.61	86.87±1.33	86.36±2.15	538	0.44	0.67	...	R

Columns are as Table 1, with the addition of the Survey identifier in column 11. These are designated with A for APOGEE DR14 (Majewski et al. 2017; Holtzman et al., in prep.), L for LAMOST (Luo et al. 2015; Xiang et al. 2017), and R for RAVE (Steinmetz et al. 2006; Kunder et al. 2017). ^aThe RV for *Gaia* DR2 1268023196461923712 comes from the APOGEE survey (that from the LAMOST survey is consistent to within a few km s⁻¹).

and those from TiO, ZrO, FeH, CaH from B. Plez (private communication).

The BACCHUS package derives the stellar atmospheric parameters - effective temperature (T_{eff}), surface gravity ($\log g$), microturbulent velocity (ξ), and iron abundance ($[\text{Fe}/\text{H}]^3$), under the assumption of local thermodynamic equilibrium (LTE)⁴ and using the standard Fe-Ionization-Excitation equilibrium technique. Under this procedure the value of T_{eff} is derived by ensuring that there is no correlation between the abundance of Fe, denoted as $\log_{10}(A_{\text{Fe}})$,

³ Chemical abundances are represented in the standard way as a logarithmic ratio of element X to element Y, relative to the Sun, $[\text{X}/\text{Y}]$, such that $[\text{X}/\text{Y}] = \log\left(\frac{N_{\text{X}}}{N_{\text{Y}}}\right)_{\text{star}} - \log\left(\frac{N_{\text{X}}}{N_{\text{Y}}}\right)_{\text{Sun}}$, where N_{X} and N_{Y} are the number of element X and element Y per unit volume respectively.

⁴ Possible non-LTE (NLTE) effects on the derived values of the atmospheric parameters and chemical abundances are not taken into account.

and the excitation potential (in eV) of the lines being used. The value of $\log g$ is determined by ensuring that there is no significant offset between the abundance of neutral Fe (Fe I) and that of singly ionized Fe (Fe II). Finally, the value of the microturbulent velocity, ξ , is derived by forcing there to be no correlation between the abundance of Fe and the reduced equivalent width (REW, defined as equivalent width divided by the wavelength of the line). These steps in the derivation of the stellar atmospheric parameters were completed using up to 90 Fe I lines and 30 Fe II lines. For more details about BACCHUS, we refer the reader to Section 2.2 of Hawkins et al. (2015).

The chemical abundances, reported as $[\text{X}/\text{H}]$, were derived for each element and each absorption feature by first fixing the stellar parameters to those derived as described above and synthesizing spectra with different values of $[\text{X}/\text{H}]$. A χ^2 minimization was done between the observed spectrum and the synthesized spectra with different $[\text{X}/\text{H}]$ values to obtain the elemental abundance. This process was

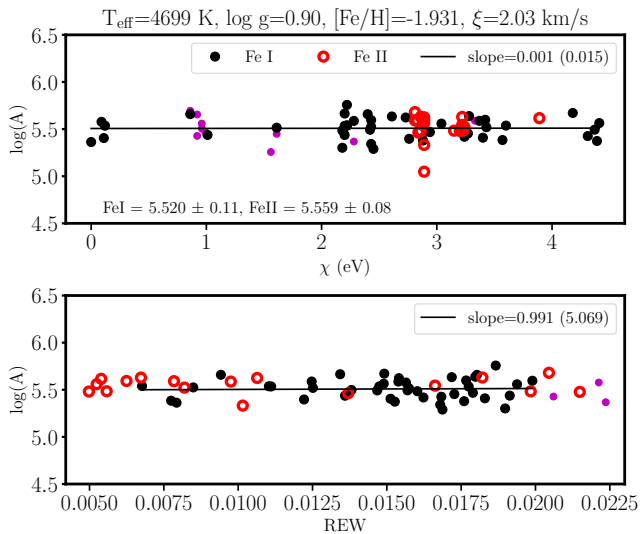


Figure 2. Illustrates the Fe excitation-ionization balance used to derive the stellar parameters for *Gaia* DR2 1508756353921427328. The upper panel shows the log of the Fe abundance, $\log_{10}(A_{\text{Fe}})$ for Fe I lines (black filled circles) and Fe II lines (open red circles) as a function of the excitation potential of the line, in eV. The lower panel shows the $\log_{10}(A_{\text{Fe}})$ for Fe I and Fe II lines as a function of reduced equivalent width, $\text{REW} = \text{EW}/\lambda$. The magenta filled circles in both panels represent lines that are stronger than ~ 120 mÅ and thus were rejected from the stellar parameter analysis.

repeated for each element and resulted in abundances for 22 species. We take the median and dispersion of the abundances derived from individual lines, divided by the square root of the number of lines used, as the quoted abundance and internal error, respectively. The abundances are scaled relative to the Sun by adopting the Solar abundances for each element from [Asplund et al. \(2005\)](#).

4 RESULTS AND DISCUSSION

4.1 Stellar Parameters and Radial Velocities

It is immediately obvious from the entries in [Tables 1 and 2](#) that there is excellent agreement between the radial velocities reported by *Gaia* and those measured by us, and those reported by other surveys. The median offset is less than 1 km s^{-1} and the dispersion is $\sim 2 \text{ km s}^{-1}$. This is reassuring, especially as the *Gaia* team cautions the use of radial velocities with high values (e.g. [Gaia Collaboration et al. 2018](#)). That said, one star, *Gaia* DR2 1508756353921427328, has a radial velocity measurement from our APO spectrum that is 6 km s^{-1} different from that reported by *Gaia*. It is hard to quantify variability and binarity with just two epochs of data; this star warrants monitoring to determine its status.

The derived values of the stellar atmospheric parameters (and the associated uncertainties) for the observed extreme-velocity candidates are given in the top 4 rows of [Table 3](#). These parameters are derived using the standard technique of Fe ionization-excitation balance (see [section 3](#) above). An illustration of the stellar parameter solution ob-

tained in this manner is shown in [Fig. 2](#) for star *Gaia* DR2 1508756353921427328. The upper panel of this figure shows the excitation balance where, for the adopted set of stellar parameters (given at the top of the figure), there is no correlation between the log of the Fe I abundance (black filled circles) and the excitation potential. The formal slope of the linear relation fit (and its standard error) is shown in the top right corner of the panel. The black line represents the linear fit to the data.

The ionization balance, namely that the abundances derived from Fe I and Fe II (red open circles) are in good agreement with each other, is also illustrated, with the actual values given in the bottom left corner of the panel. The lower panel of [Fig. 2](#) shows the log Fe abundance for both Fe I (black filled circles) and Fe II (red open circles) as a function of the reduced equivalent width. This lower panel is used to constrain the value of the microturbulent velocity, ξ . The magenta filled circles in both panels of [Fig. 2](#) represent very strong lines (above ~ 120 mÅ EW) which are excluded from the analysis, as they may no longer be on the linear part of the curve of growth.

The resultant typical internal uncertainties of our derived atmospheric parameters are $\sim 75 \text{ K}$, 0.30 dex, 0.10 dex, and 0.15 km s^{-1} for T_{eff} , $\log g$, $[\text{Fe}/\text{H}]$, and ξ , respectively. The results from our stellar parameter analysis indicate that all of the extreme-velocity candidates observed with APO are metal-poor ($-2 < [\text{Fe}/\text{H}] < -1.0$) giant stars, consistent with their location in the colour-absolute magnitude diagram shown in [Marchetti et al. \(2018\)](#). This conclusion is also consistent with the analysis of the colour-absolute magnitude diagram of a differently defined extreme-velocity sample by [Hattori et al. \(2018\)](#).

It is important to note that Fe abundances from metal-poor giant stars suffer from NLTE effects and these can cause the Fe excitation-ionization balance procedure to produce T_{eff} values that are too small compared to other methods (e.g. [Frebel et al. 2013](#), and references therein). Thus we compare our results with the photometric T_{eff} values from the recent release of the *Gaia* data. These photometric T_{eff} values are also tabulated in [Table 3](#). The excitation balance T_{eff} are, on average offset from the *Gaia* photometric T_{eff} by -173 K (with the excitation balance T_{eff} being smaller, as expected from NLTE effects) with a dispersion of 183 K . Even though the *Gaia* photometric T_{eff} have very large uncertainties in some cases for these stars, we have redone the stellar parameter analysis fixing the effective temperature to the photometrically derived values from *Gaia*. We found that while the derived value of $[\text{Fe}/\text{H}]$ can change by as much as $+0.30$ dex, we are still led to the conclusion that these HVS candidate stars are metal-poor ($[\text{Fe}/\text{H}] < -1.0$ dex) giants.

As noted earlier, in addition to the extreme-velocity candidates we observed with APO, we identified four other candidates from [Marchetti et al. \(2018\)](#) in the public databases of three large spectroscopic surveys (APOGEE, RAVE, and LAMOST) and thus these stars also have derived stellar parameters. Specifically, *Gaia* DR2 1268023196461923712 has additional spectra from both the APOGEE and LAMOST surveys. The published radial velocity for this star in each of the two surveys agree to within a few km s^{-1} and both are in good agreement with that of *Gaia*. The LAMOST survey reports that this star has $T_{\text{eff}} = 4893 \pm 10 \text{ K}$, $\log g = 2.04 \pm 0.01$ dex and

Table 3. Stellar parameters and chemical abundances for 5 Candidate Extreme-velocity Stars

Star	1508756353921427328	1364548016594914560	4593398670455374592	4248140165233284352	2233912206910720000
T_{eff} (K)	4699 ± 85	4640 ± 98	4868 ± 65	4718 ± 49	5070 ± 7
$T_{\text{eff,phot}}^a$ (K)	4967^{+75}_{-57}	4813^{+220}_{-261}	5469^{+774}_{-441}	4858^{+89}_{-72}	5158^{+802}_{-79}
$\log g$ (cgs)	0.90 ± 0.43	1.37 ± 0.49	1.47 ± 0.28	1.41 ± 0.36	1.30 ± 0.26
[Fe/H]	-1.93 ± 0.09	-1.21 ± 0.12	-1.67 ± 0.13	-1.82 ± 0.15	-1.72 ± 0.16
ξ (km s^{-1})	2.04 ± 0.16	1.77 ± 0.10	1.58 ± 0.24	1.87 ± 0.18	2.28 ± 0.14
[Na/Fe]	0.21 ± 0.09	-0.11 ± 0.05	0.53 ± 0.12	0.34 ± 0.02	... \pm ...
[Mg/Fe]	0.64 ± 0.03	0.23 ± 0.07	0.58 ± 0.06	0.65 ± 0.13	0.31 ± 0.13
[Al/Fe]	... \pm ...	0.33 ± 0.10	0.07 ± 0.10	... \pm \pm ...
[Si/Fe]	0.58 ± 0.05	0.08 ± 0.05	0.37 ± 0.05	0.56 ± 0.05	0.77 ± 0.08
[K/Fe]	1.19 ± 0.10	0.75 ± 0.10	... \pm ...	1.38 ± 0.10	... \pm ...
[Ca/Fe]	0.50 ± 0.03	0.26 ± 0.04	0.50 ± 0.03	0.53 ± 0.03	0.54 ± 0.04
[Sc/Fe]	0.17 ± 0.05	0.20 ± 0.02	0.26 ± 0.04	0.24 ± 0.08	0.08 ± 0.13
[Ti/Fe]	0.29 ± 0.03	0.32 ± 0.02	0.23 ± 0.03	0.36 ± 0.04	0.16 ± 0.06
[V/Fe]	0.23 ± 0.03	0.07 ± 0.04	-0.28 ± 0.14	0.29 ± 0.10	... \pm ...
[Cr/Fe]	-0.11 ± 0.06	0.10 ± 0.04	-0.30 ± 0.06	-0.03 ± 0.08	0.70 ± 0.03
[Mn/Fe]	-0.23 ± 0.09	-0.27 ± 0.02	-0.28 ± 0.06	-0.23 ± 0.06	-0.13 ± 0.10
[Co/Fe]	0.12 ± 0.06	0.13 ± 0.03	-0.00 ± 0.03	0.31 ± 0.06	1.30 ± 0.10
[Ni/Fe]	0.03 ± 0.05	-0.04 ± 0.03	0.03 ± 0.05	0.13 ± 0.04	0.15 ± 0.07
[Cu/Fe]	-0.33 ± 0.03	-0.38 ± 0.15	-0.99 ± 0.17	-0.19 ± 0.13	0.31 ± 0.10
[Zn/Fe]	-0.11 ± 0.01	-0.13 ± 0.11	0.06 ± 0.04	0.00 ± 0.01	0.16 ± 0.10
[Sr/Fe]	0.10 ± 0.10	-0.41 ± 0.10	... \pm ...	0.22 ± 0.10	... \pm ...
[Y/Fe]	-0.11 ± 0.08	-0.20 ± 0.07	-0.11 ± 0.05	-0.18 ± 0.10	-0.14 ± 0.01
[Zr/Fe]	0.23 ± 0.13	0.37 ± 0.10	0.59 ± 0.13	0.90 ± 0.03	0.77 ± 0.10
[Ba/Fe]	-0.02 ± 0.12	0.18 ± 0.12	0.56 ± 0.03	0.02 ± 0.13	-0.15 ± 0.15
[La/Fe]	0.28 ± 0.03	0.26 ± 0.04	0.16 ± 0.06	0.66 ± 0.07	0.71 ± 0.08
[Nd/Fe]	0.31 ± 0.02	0.28 ± 0.03	0.17 ± 0.03	0.74 ± 0.06	0.43 ± 0.08
[Eu/Fe]	0.77 ± 0.10	... \pm ...	0.34 ± 0.10	0.70 ± 0.10	1.11 ± 0.29

NOTE: The T_{eff} , $\log g$, [Fe/H], ξ , and [X/Fe] for 22 elements are tabulated here for each of the 5 stars in this work. We note that the uncertainty on each abundance represents only the internal error and is defined as the line-to-line dispersion of the abundance divided by the square root of the number of lines. When only 1 line can be measured for an element the assumed internal uncertainty is conservatively 0.10 dex. ^a We also report the photometric T_{eff} based on photometry from the *Gaia* DR2 (BP-RP) colour (for more details consult [Andrae et al. 2018](#)).

[Fe/H] = -1.58 ± 0.01 dex while the APOGEE survey reports that the same star has $T_{\text{eff}} = 4924 \pm 100$ K, $\log g = 2.38 \pm 0.11$ dex and [Fe/H] = -1.62 ± 0.07 dex. The three remaining stars were serendipitously observed by the RAVE survey. All three have RAVE radial velocities that agree, to within a few km s^{-1} , with the values from *Gaia*. Only two of the three (*Gaia* DR2 6639557580310606976 and *Gaia* DR2 5212817273334550016) have published values of the stellar parameters: both are metal-poor giant stars with [Fe/H] = -1.49 ± 0.17 for *Gaia* DR2 6639557580310606976 and [Fe/H] = -1.80 ± 0.14 dex for *Gaia* DR2 5212817273334550016.

Overall, our analysis shows that these extreme-velocity candidates, selected from [Marchetti et al. \(2018\)](#), are metal-poor giant stars, with iron abundances typical of the stellar halo, albeit moving with higher than typical halo velocities. With the stellar parameters in hand, we next turn to determination of the chemical abundance patterns, treating the different elemental families in turn: α -elements (section 4.2), odd-Z elements (section 4.3), Fe-peak elements (section 4.4), and, finally, neutron-capture elements (section 4.5). This exploration should help discern if these stars have originated in the Galactic centre, the LMC, the Galactic disc(s) or are indeed simply part of the stellar halo.

4.2 α elements: Mg, Ti, Si, Ca

The α elements are those which are formed via successive addition of helium nuclei (α -particles) during the later stages of (quasistatic) nuclear fusion in the inner regions of evolved massive stars. These elements include Magnesium (Mg), Titanium (Ti), Silicon (Si), Calcium (Ca) and Oxygen (O)⁵. The α elements are primarily dispersed into the interstellar medium (ISM) by core-collapse (Type II) supernovae, which occur rapidly after the birth of the progenitor massive star. Core-collapse supernovae produce relatively little iron, so that early on, shortly after the onset of star formation, the ISM, and any newly formed stars, will be enriched to high values of $[\alpha/\text{Fe}]$. The explosive nucleosynthesis inherent in Type Ia supernovae creates a high yield of iron, but only after a significant delay time following the birth of the progenitor (lower mass) stars. Stars that form later, after incorporation of iron from Type Ia supernovae into the ISM, will show lower values of $[\alpha/\text{Fe}]$. The ratio of α elements to Fe is therefore sensitive to the star-formation history and past enrichment of the gas from which the star formed (e.g.

⁵ We attempted to measure O for each star using the forbidden O I line at 6300 Å but in all cases the line could not be fit acceptably.

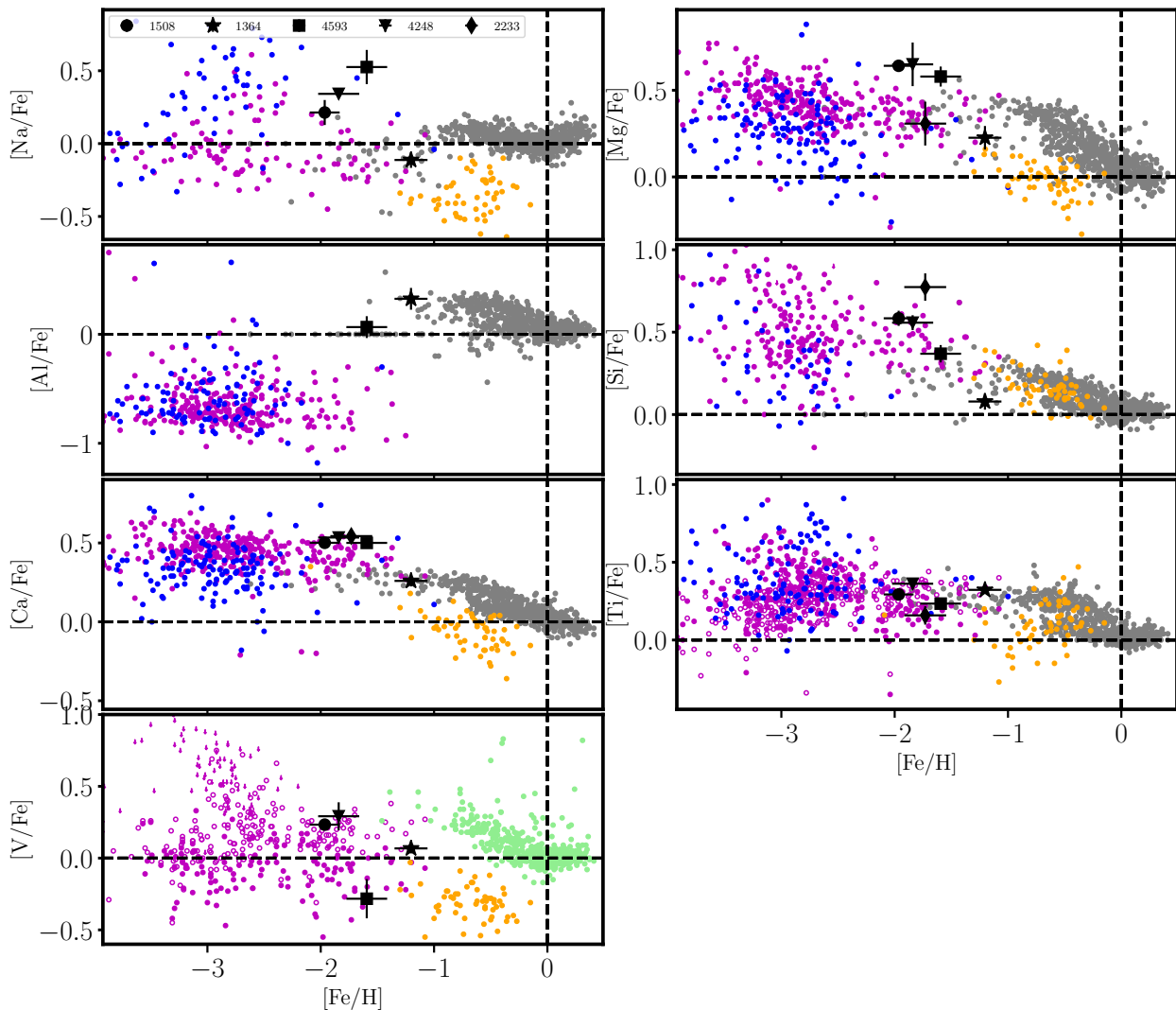


Figure 3. Illustrates the $[X/Fe]$ ratios of the program stars (black filled symbols) as a function of $[Fe/H]$ for Na, Al, Ca, and V from top to bottom, respectively, on the left and Mg, Si, and Ti from top to bottom, respectively, on the right. These elements largely represent the α and odd-Z elements. The background displays abundances for the disc (including thin and thick disc) from [Bensby et al. \(2014\)](#), gray filled circles) and [Battistini & Bensby \(2016\)](#), light green). In addition, abundances in each chemical species (where defined) for the halo are also shown, taken from [Roederer et al. \(2014\)](#), magenta filled circles for neutral lines, and magenta open circles for ionized lines,) and [Yong et al. \(2013\)](#), blue filled circles). We also plot the chemical abundances from stars in the inner disc and/or bulge area of the LMC from [Van der Swaelmen et al. \(2013\)](#), orange filled circles). Arrows represent upper limits and are shown from the results of [Roederer et al. \(2014\)](#).

[Gilmore & Wyse 1998](#); [Matteucci & Recchi 2001](#); [Nomoto et al. 2013](#)).

This last point makes α elements key species that can allow us to distinguish the environment within which the rare extreme-velocity stars may have originated. Stars belonging to the local Galactic thin disc, thick disc and halo have different distributions in the α elements as a function of metallicity. Fig. 3 shows the $[X/Fe]$ abundances for the α elements, including Mg, Ti, Si, and Ca, as a function of $[Fe/H]$ for the extreme-velocity stars observed in this work (black filled symbols, identified on the plots). For reference, we also show the $[X/Fe]$ abundances for the local Galactic thin disc and thick disc taken [Bensby et al. \(2014\)](#), gray filled circles) and [Battistini & Bensby \(2016\)](#), light green filled cir-

cles, for Vanadium only) and for the stellar halo, taken from [Yong et al. \(2013\)](#), blue filled circles) and [Roederer et al. \(2014\)](#), magenta filled circles for neutral lines, and magenta open circles for ionized lines).

We note here that the uncertainties in abundance ratios that are reported in Table 3 are only internal. There are very likely systematic uncertainties for each element in addition to the internal uncertainties. The level of those systematics is difficult to assess with few stars observed with APO ARCES that are also in common with the literature sources used to represent the chemical composition of the stellar halo ([Yong et al. 2013](#); [Bensby et al. 2014](#); [Roederer et al. 2014](#)), disc ([Bensby et al. 2014](#); [Battistini & Bensby 2016, 2015](#)), and LMC ([Van der Swaelmen et al. 2013](#)). We

assume the level of the systematic uncertainty in the abundances (specifically $[\text{Fe}/\text{H}]$) is on the order of ~ 0.10 dex. This assumption is based on the typical offsets between the BACCHUS derived $[\text{Fe}/\text{H}]$ and the adopted values for metal-poor ($[\text{Fe}/\text{H}] < -1.0$ dex) *Gaia* FGK benchmark stars from [Jofré et al. \(2014\)](#) and [Hawkins et al. \(2016\)](#). In addition, we have observed with APO ARCES a couple of metal-poor ($[\text{Fe}/\text{H}] \sim -0.70$ dex) disc stars that are in common with [Bensby et al. \(2014\)](#) for an unrelated forthcoming study. We found an offset in $[\text{Fe}/\text{H}]$ of ~ 0.10 dex similar to the assumed value.

As we concluded above, all of the candidate extreme-velocity stars observed are metal-poor giant stars with $-2 < [\text{Fe}/\text{H}] < -1$ dex. This puts these stars near the peak of the metallicity distribution of the inner Galactic halo (expected to be at $[\text{Fe}/\text{H}] \sim -1.5$, e.g. [Chiba & Beers 2000](#)). In addition, it is clear that in almost all α elements these metal-poor giant stars show enhanced ratios of α/Fe relative to the Sun ($[\alpha/\text{Fe}] > 0$), albeit with relatively large scatter. The level of enhancement in $[\alpha/\text{Fe}]$ we find is typical of that found in the Galactic stellar halo. It is interesting to note that the least metal-poor star, *Gaia* DR2 1364548016594914560, is only marginally enhanced in Mg and Si compare to the other Ca and Ti but still falls in the scatter of typical stellar halo stars. The more metal-rich of these stars could also be consistent with being runaway stars from the metal-weak thick disc. The additional extreme-velocity candidate from the APOGEE survey lacks individual elemental abundances but also shows overall α enhancement at a level typical of halo stars in that survey.

The chemical distribution in the α elements effectively rules out that these stars have originated in the LMC, where the expected signature would be for the stars to be more metal-rich ($-1.5 < [\text{Fe}/\text{H}] < 0.0$ dex) and more depleted in the α elements (e.g. [Van der Swaelmen et al. 2013](#)). Similarly, the chemical distribution in the α elements effectively rules out an origin in the Galactic centre, where it would be expected that the stars should be significantly more metal-rich ($[\text{Fe}/\text{H}] > -0.8$) and more enhanced in the α elements (e.g. [McWilliam 2016](#)). Instead the chemical distribution in the α elements of these extreme velocity stars appear most similar to those seen in typical halo stars.

4.3 Odd-Z Elements: Na, Al, V, Cu, Sc

The odd-Z elements are produced in a variety of ways. As such, we will discuss each separately below.

Na:

Sodium (Na) is thought to be produced both during carbon burning and through the NeNa cycle during H-shell burning in the post main-sequence phase of low- and intermediate-mass stars (e.g. [Samland 1998](#)). It is dispersed into the interstellar medium by both SNII and partially through the evolution of AGB stars ([Nomoto et al. 2013](#)). SNIa do not efficiently produce Na compared to Fe and thus $[\text{Na}/\text{Fe}]$ is expected to decrease towards higher metallicities. Published results in the literature show that $[\text{Na}/\text{Fe}]$ as a function of $[\text{Fe}/\text{H}]$ for stars in the Galactic disc shows a banana shape, while in the Galactic halo Na becomes overabundant when the abundances are derived in LTE (blue points in Fig. 3). These values slightly decrease when NLTE (magenta points in Fig. 3) is considered, as by [Roederer et al. \(2014\)](#). On the

other hand, $[\text{Na}/\text{Fe}]$ in the LMC has been measured and is thought to be significantly lower than the Galactic disc or halo at the same metallicities (e.g. [Van der Swaelmen et al. 2013](#)). The HVS candidate stars mostly display super-solar ratios of $[\text{Na}/\text{Fe}]$, with one star (*Gaia* DR2 1364548016594914560) being closer to solar values. Much like the case of the α elements, the Na abundances of these HVS candidate stars mostly follow those of the Galactic halo, albeit with a large scatter.

Al:

Similarly to Na, aluminum (Al) is produced in carbon burning in post main-sequence evolution. However, unlike Na, it is also produced in the MgAl cycle (e.g. [Samland 1998](#)). It is mostly dispersed into the interstellar medium via SNII but also through the evolution of AGB stars. The observed ratio of Al to Fe follows the patterns seen for Mg, Si, Ca, and O, in that at high metallicity ($[\text{Fe}/\text{H}] > -1$) it increases with decreasing metallicity. This is why Al is often thought of as a ‘mild’ α element. However, unlike the α elements, at lower metallicity $[\text{Al}/\text{Fe}]$ is observed to decrease with decreasing metallicity, reaching a plateau at sub-solar values, a trend also expected by models (e.g. [Kobayashi et al. 2006](#); [Nomoto et al. 2013](#)). We could measure Al in only two of the five observed stars (Fig. 3) and found, in both cases, that the $[\text{Al}/\text{Fe}]$ value lies within the scatter of typical halo stars in the metallicity range of $-1 < [\text{Fe}/\text{H}] < -2$ dex.

V:

The nucleosynthesis pathway for the production of vanadium (V) is not well understood. This can be seen in the rather poor agreement between the theoretical expectation for the behaviour of $[\text{V}/\text{Fe}]$ as a function of metallicity and the data (see, for example, Fig. 10 of [Nomoto et al. 2013](#)). Regardless of this fact, we can empirically compare the derived values of $[\text{V}/\text{Fe}]$ for our stars with those from known populations. Fig. 3 shows the derived values of $[\text{V}/\text{Fe}]$ as a function of metallicity for the extreme-velocity stars (black) compared to the Galactic disc (light green circles [Battistini & Bensby 2016](#)), the Galactic halo ([Yong et al. 2013](#); [Roederer et al. 2014](#)), and the LMC ([Van der Swaelmen et al. 2013](#)). The candidate extreme-velocity stars have a wide range in $[\text{V}/\text{Fe}]$, again consistent with the large scatter observed for the Galactic halo.

Cu:

Copper (Cu) is an odd-Z element that is thought to be largely produced via SNIa and hypernovae but is also produced by secondary phenomena in massive stars and the weak s-process (e.g. [Mishenina et al. 2002](#)). Like many elements, the exact nucleosynthetic process that forms Cu is still under debate (e.g. [Andrievsky et al. 2018](#)). As shown in Fig. 4, previous surveys found a large scatter in $[\text{Cu}/\text{Fe}]$ at the metallicities of our stars, and similar low values in the LMC and stellar halo. Again, the stars in our sample fit within the scatter of the stellar halo, but Cu does not allow us to distinguish between stars born in the Galactic disc, halo or LMC.

Sc:

Scandium (Sc) is an odd-Z element that, similarly to vanadium, has a poorly understood nucleosynthesis production mechanisms. This is evident by the large discrepancies be-

tween the theoretically computed and observed trends of $[\text{Sc}/\text{Fe}]$ as a function of $[\text{Fe}/\text{H}]$ (e.g. Kobayashi et al. 2006; Nomoto et al. 2013). As seen in Fig. 4 stars belonging to either the LMC or Galactic disc show $[\text{Sc}/\text{Fe}]$ increasing with decreasing metallicity, with $[\text{Sc}/\text{Fe}]$ lower in the LMC at fixed metallicity compared to the Galactic disc (Van der Swaelmen et al. 2013).

On the other hand, stars in the Galactic halo have $[\text{Sc}/\text{Fe}]$ values which are either slightly enhanced (Yong et al. 2013) or solar (Roederer et al. 2014) though with large intrinsic scatter. The candidate extreme-velocity stars are all enhanced in $[\text{Sc}/\text{Fe}]$ at levels consistent with the Galactic halo but not with the LMC.

4.4 Fe-peak elements: Cr, Mn, Co, Ni, Zn

Unlike the α or odd-Z elements, the Fe-peak elements, such as chromium (Cr), scandium (Sc), manganese (Mn), cobalt (Co), nickel (Ni), and zinc (Zn), are formed through a variety of paths (Iwamoto et al. 1999; Kobayashi et al. 2006) but are largely dispersed into the interstellar medium in a similar way as iron. As such, these Fe-peak elements largely track the abundance of Fe. At the metallicity range of the candidate extreme-velocity stars ($-2 < [\text{Fe}/\text{H}] < -1$), $[\text{Co}/\text{Fe}]$ and $[\text{Zn}/\text{Fe}]$ increase with decreasing metallicity while $[\text{Ni}/\text{Fe}]$, and $[\text{Cu}/\text{Fe}]$ remain approximately constant. The other Fe-peak elements (Mn and Cr) display $[\text{X}/\text{Fe}]$ values which decrease with decreasing metallicity.

More specifically, Fig. 4 shows that $[\text{Cr}/\text{Fe}]$ and $[\text{Ni}/\text{Fe}]$ are approximately constant, at close to the solar value, for stars in the Galactic disc(s). However, in the Milky Way halo, $[\text{Cr}/\text{Fe}]$ decreases with decreasing metallicity, with large scatter (e.g. Yong et al. 2013; Roederer et al. 2014). It should however be noted that abundances based on Cr II measured by Roederer et al. (2014) are offset from the Cr I abundances of the same authors, which agree with the Cr reported in Yong et al. (2013). In the disc of the LMC, $[\text{Cr}/\text{Fe}]$ varies little with metallicity (similar to the lack of trend seen in the Milky Way disc) but at lower values than in the Galactic disc and with large scatter. The Ni and Cr abundances of the candidate extreme-velocity stars are consistent with the Galactic halo or, in the case of the most metal-rich of the observed HVS candidates (*Gaia* DR2 1364548016594914560), with the Galactic thick disc or even with the LMC.

Mn is a Fe-peak element and its production is thought to be similar Ni (e.g. Kobayashi & Nakasato 2011), however the observed chemical trend in the Galactic disc and halo as a function of $[\text{Fe}/\text{H}]$ is different than Ni. This unexpected trend is not well understood. However, Battistini & Bensby (2015), found that the $[\text{Mn}/\text{Fe}]$ ratio is constant at low metallicity (rather than decreasing) if NLTE calculations are considered. Since we compute all elemental abundances assuming LTE, we only compare the LTE calculations for Mn (and all elements) from other surveys of the Galactic disc(s), halo and LMC, to our HVS candidate stars. Mn shows a decreasing trend with decreasing metallicity through the Galactic disc(s) and halo. The HVS candidate stars observed in this study follow this expected trend and are consistent with originating in the Milky Way. The HVS candidate stars show trends in each of the Fe-peak elements that are consistent with the Galactic halo (low metallicity and large abundance scatter) in all Fe-peak elements. How-

ever, they are inconsistent with the Galactic disc(s) in Fe, Mn and Co and inconsistent with the LMC disc in Fe, Co and Ni.

4.5 Neutron capture elements: Sr, Y, Zr, Ba, La, Nd, Eu

The neutron capture elements are generally split into two separate groups, namely the slow (s-process) and rapid (r-process) neutron capture elements. The s-process elements are often subdivided into a light s-process group comprised of strontium (Sr), yttrium (Y), and zirconium (Zr) and heavy s-process group made of barium (Ba), lanthanum (La), neodymium (Nd) among others. The exact nucleosynthetic production channel is marginally constrained for some elements such as Ba but not well understood for others (e.g. the r-process element europium, Eu). For example, Ba is largely s-process in origin and is thought to be created primarily in AGB stars and ejected through stellar winds. Other s-process elements (e.g. Sr and Zr) are also thought to be largely created by AGB stars while pure r-process elements (e.g. Eu) may be created by more violent events such as the merger of binary neutron stars. The relative abundances of the neutron-capture elements contain unique insight into the environments of the extreme-velocity stars at their births.

Fig. 5 shows that all the candidate extreme-velocity stars have abundances in the light s-process elements that are consistent with the metal-poor halo (or thick disc for the more metal-rich candidates), showing near solar values in $[\text{Sr}/\text{Fe}]$ and $[\text{Y}/\text{Fe}]$ but enhanced in $[\text{Zr}/\text{Fe}]$. These values are, however, inconsistent with those seen in thin disc stars or the disc of the LMC, which would, for example, require both a high metallicity and significantly lower $[\text{Zr}/\text{Fe}]$. The candidate extreme-velocity stars are also all consistent with the metal-poor halo (or thick disc) in the heavy s-process elements, showing enhanced values for $[\text{La}/\text{Fe}]$ and $[\text{Nd}/\text{Fe}]$ but mostly near solar values for $[\text{Ba}/\text{Fe}]$. However, *Gaia* DR2 4593398670455374592 has a higher $[\text{Ba}/\text{Fe}]$ value and if it were at higher metallicity it could be consistent with stars in the disc of the LMC. The only r-process element we currently measure is Eu and again the extreme-velocity stars lie within the scatter of the stellar halo.

4.6 Origins of the Hypervelocity Candidate Stars: A Chemical Perspective

The elemental abundances we reported above for five of the 28 HVS candidates from Marchetti et al. (2018) which those authors find to have high probability of being unbound to the Milky Way, indicate that these stars do not originate in either the Galactic thin disc or the LMC. This is likely also the case for the HVS candidates that are metal-poor giants found in common with several large spectroscopic surveys. This conclusion is based largely on the abundances of the α (Mg, Ca, Ti), odd-Z (Na, V, Sc,), Fe-peak (Fe, Co, Mn), and neutron capture (Zr, Ba) elements. Rather, in all elements studied, these fast-moving metal-poor giant stars show abundances typical of Galactic halo stars, with the caveat that the most metal-rich of these stars could have originated in the metal-weak thin disc (e.g. Beers et al.

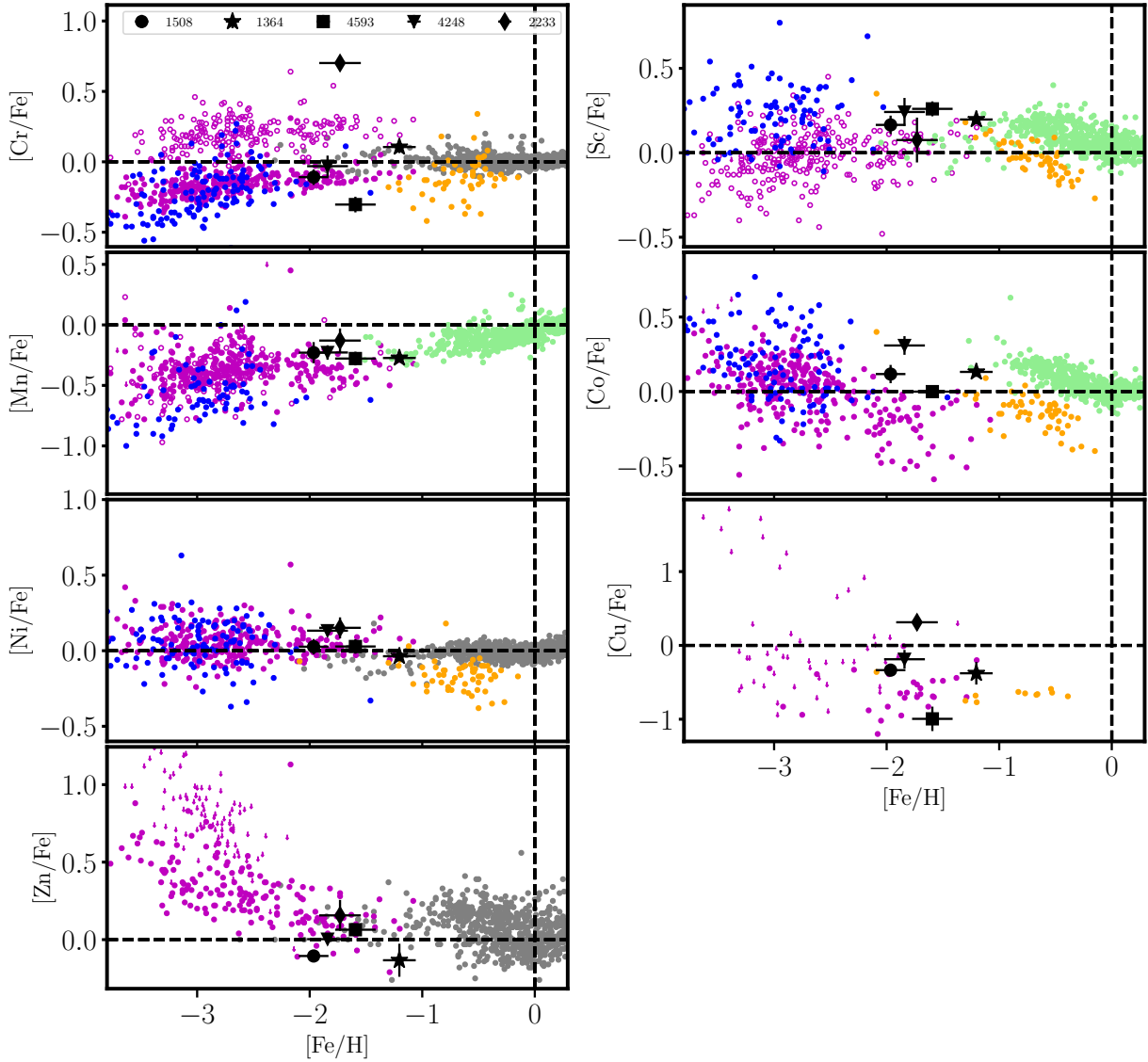


Figure 4. The $[X/Fe]$ ratios of the program stars (black filled symbols) as a function of $[Fe/H]$ for Cr, Mn, Ni, and Zn from top to bottom, respectively on the left and Sc, Co, and Cu from top to bottom, respectively on the right. These largely represent the Fe-peak elements. The symbols are the same as in Fig. 3.

2002; Ruchti et al. 2011), although its high velocity suggests that it may simply be the high-velocity tail of the stellar halo. With the data presented above in Figs. 3, 4, and 5 in mind, we now put this result into the broader context of the origins of HVS.

Hills' Mechanism:

One of the primary mechanisms proposed for the production of stars moving well in excess of the Galactic escape velocity is a triple-body encounter between a binary stellar system and a massive object such as the Milky Way's supermassive black hole or intermediate mass black holes (Hills 1988; Yu & Tremaine 2003; Gualandris & Portegies Zwart 2007). This mechanism is the expected process involved in the creation of most of the known and confirmed early-type massive, and hence young, HVSs (Brown 2015).

Some of the extreme-velocity stars observed in this work - all late-type, low mass stars - have inferred orbits which are consistent with a high likelihood of passing within 1 kpc of the Galactic center (Marchetti et al. 2018). If these stars actually did originate close to the Galactic centre and had been ejected by the purely dynamical Hills' mechanism then their chemical abundance pattern should match that of low-mass stars in the inner Galaxy. Figs 3, 4, and 5 all demonstrate that this is not the case. Low-mass giant stars in the Galactic centre region are generally metal-rich ($[Fe/H] > -1.0$) and enhanced in the α elements (e.g. McWilliam 2016, and references therein). Further, the chemical patterns of these three candidates which have derived orbits that intersect the Galactic centre also do not resemble those of stars in the inner regions of the thin disc. Therefore, we conclude that it is very

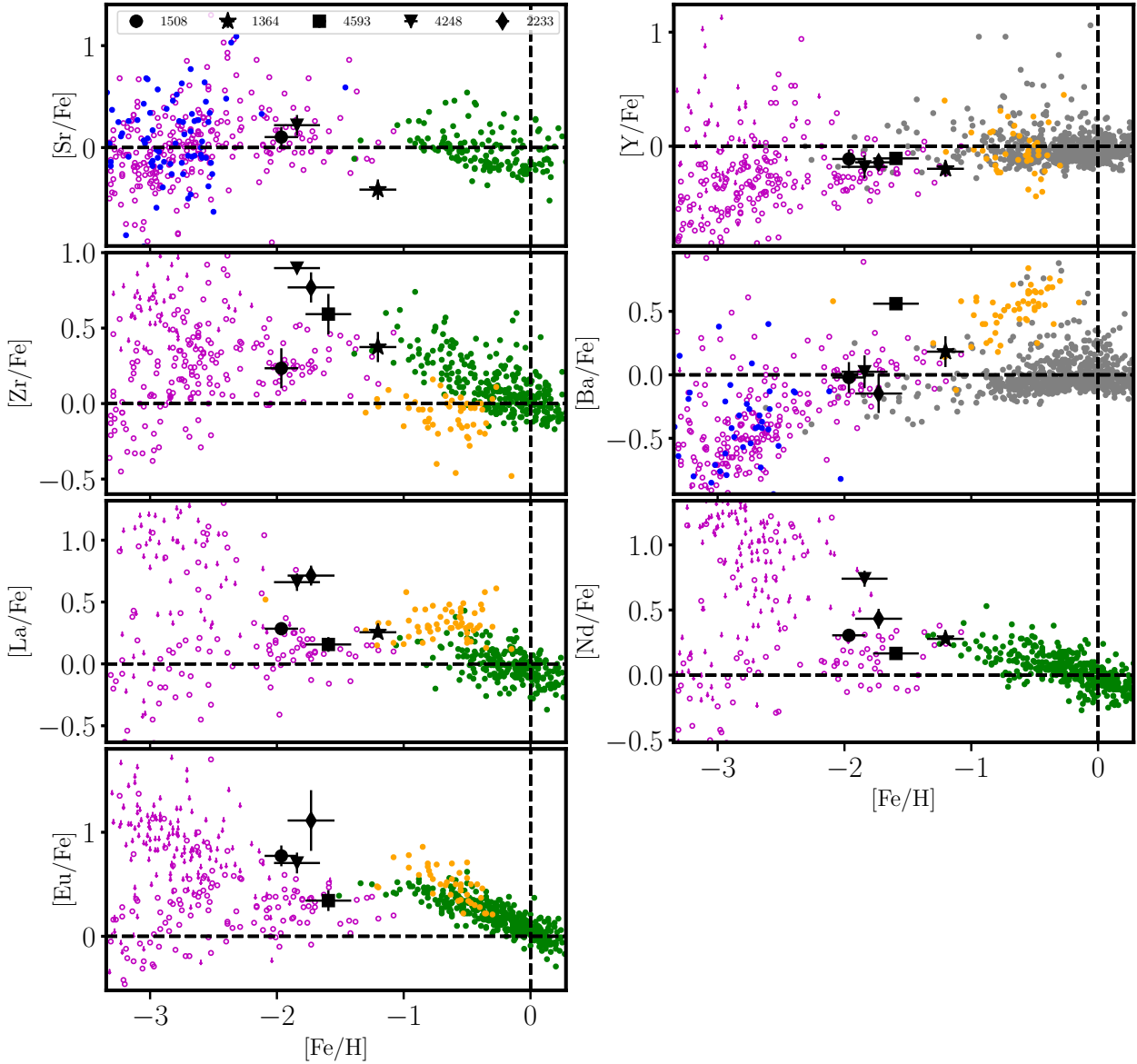


Figure 5. $[X/Fe]$ as a function of metallicity for Sr, Zr, La, and Eu from top to bottom, respectively on the left and Y, Ba, and Nd from top to bottom, respectively on the right. These largely represent the neutron capture elements. The symbols are the same as Fig. 3 with additional data for the disc taken from Battistini & Bensby (2015, green).

unlikely that these stars have actually originated close to the Galactic centre, a requirement for the Hills' mechanism⁶.

Hypervelocity Stars from the Large Magellanic Cloud or Tidal Debris?:

Another potential origin for HVSs that has been proposed in the literature is as runaway stars from the LMC or tidal debris. This idea was first proposed by Edelmann et al. (2005) who noted that one HVS was less than 20 deg from the centre of the LMC. The idea was then extended by Boubert &

Evans (2016) and Boubert et al. (2017) who predicted the kinematic and spatial properties that would result if B-type HVS were runaway stars from the LMC, and found agreement with the observed population. Most recently, Erkal et al. (2018) have shown, using *Gaia* DR2, that at least one of the known and confirmed HVSs does indeed come from the LMC. With this in mind, we assess whether the metal-poor HVS candidates in this work are consistent with an origin in the LMC.

If these HVS candidate stars were coming from the LMC then (1) their orbits should trace back to the LMC and (2) their chemistry should resemble the (disc component) of the LMC. Marchetti et al. (2018) has noted that some of their candidates, specifically those with low probability of crossing

⁶ Giant stars have sufficiently large radii that they are unlikely to be in a tight enough orbit for Hills' mechanism (e.g. Bromley et al. 2006; Kenyon et al. 2008).

the Galactic disc ($P_{MW} < 0.50$), may have an extragalactic origin, such as being ejected from the LMC or tidally stripped debris. Again the detailed chemical abundance distributions provide a means to distinguish between an origin in the Milky Way and an extragalactic origin. We determine whether the chemical distribution of the HVSs candidate stars are consistent with the LMC in Figs 3, 4, and 5. It is clear that the HVSs have chemical abundance signatures that do not match those of the LMC in various elements, including Na, Mg, Ca, Sc, Co, Ni, and Zr. More specifically, the candidate extreme-velocity stars are more enhanced in these elements than are stars in the LMC. This rules out an origin in the LMC. Tidal debris from other satellite systems could have low metallicity, as observed for the candidate HVSs, but would be expected to have the low values of the abundance ratios [Mg, Si, Ca, Ti/Fe] found in old, low-mass stars in present-day dwarf galaxies, in contrast to the enhanced values we observe.

Are these Stars Really Unbound?:

Hattori et al. (2018) compute the production rates of HVSs from globular clusters, through either ejection of the binary companion in a Type Ia supernova or the interaction between a binary star system and an intermediate mass black hole. Interestingly, they found that the rate predicted is a couple of orders of magnitude too low to replenish the population of HVSs should they actually escape from the Galaxy. This shortfall led them to conclude that, regardless of how the HVS candidates achieved their high velocities, they are in fact not escaping, but are bound to the Galaxy. Our results add a new dimension, that of the chemical signature, to this argument.

Firstly, their chemical composition indicates that the extreme velocity stars studied here most closely resembles the Galactic halo. In addition, some stars, generally referred to as second generation, in globular clusters are known to display an anti-correlation between Mg and Al (e.g. Bastian & Lardo 2017). This would make these globular cluster stars distinguishable from field stars because they have high [Al/Fe] but low [Mg/Fe], thereby having a significantly higher [Al/Mg] ratio compared to field stars. However, for two of the three stars where Al is measured, the [Al/Fe] is not high and the [Mg/Fe] is enhanced, suggesting that these stars may just be regular field halo or are former members of the first-generation of a globular cluster, which do not show a Mg-Al anti-correlation.

Furthermore, in both HVSs candidate samples from Hattori et al. (2018) and Marchetti et al. (2018), there are similar numbers of extreme-velocity stars with positive and negative RVs. All of these points taken together indicate that these HVSs candidate stars are simply just typical bound halo stars which are at the high speed tail of the velocity distribution of the stellar halo.

5 SUMMARY

Hypervelocity stars are intriguing objects that are moving faster than the escape speed of the Milky Way at their observed location and are thus unbound. These rare stars were first proposed as the ‘smoking-gun’ evidence for a super-massive black hole at the Galactic Centre by Hills (1988) and massive, young HVSs were first discovered observation-

ally in 2005 (Brown et al. 2005). With exquisite astrometric data from the *Gaia* second data release, more than 40 late-type (FGK-type) hypervelocity star candidates have been proposed (Marchetti et al. 2018; Boubert et al. 2018; Hattori et al. 2018). In this paper, we report the first spectroscopic followup and chemical characterisation of a subsample of newly proposed HVS candidates. We observed five HVS candidates from Marchetti et al. (2018) with the high-resolution ARCES spectrograph on the 3.5m telescope at the Apache Point Observatory. The observational properties of these stars can be found in Table 1. In addition to these observed targets, four more were found to be serendipitously observed by the RAVE, APOGEE, and LAMOST spectroscopic surveys.

The spectra from the APO were processed in the standard way (see section 3 for more details). Our first aim was to confirm the RV of these fast-moving stars, which are often very large ($RV \geq 300 \text{ km s}^{-1}$). On average the RV measured in our work using APO and that from *Gaia* agree to within $\sim 1 \text{ km s}^{-1}$ with a dispersion of 2 km s^{-1} . This encouraging result indicates that *Gaia* is able to measure accurate RVs, including high RV, for stars as dim as $G \sim 13.5 \text{ mag}$.

We then completed an extensive stellar atmospheric and chemical characterisation of the five observed HVS candidates and found that all five HVS candidates are metal-poor giants. This implies a dramatically different parent population from that of the known massive O- and B-type HVSs. Further, the HVS candidate stars that we identified as serendipitously observed in published large surveys are also metal-poor giant stars though their chemical detailed chemistry is unknown in most cases. The chemical abundance patterns we derived for the five stars observed with APO comprised 22 species, including Mg, Ti, Si, Ca (α group), Fe, Ni, Co, Cr, Sc, Mn (Fe-peak), Na, Al, V, Cu (odd-Z group), and Sr, Y, Zr, Ba, La, Nd, Eu (Neutron capture). In all chemical elements studied, the HVS candidate stars match typical Galactic halo stars and do not resemble stars in any of the inner Galactic bulge/disc, outer disc near the Sun or the LMC. We conclude that these stars are most likely just bound halo stars that are at the tail of its velocity distribution. A similar conclusion was reached by Boubert et al. (2018) on pure dynamical grounds. These results suggest that the Milky Way escape velocity is higher than previously estimated (Piffl et al. 2014; Williams et al. 2017), and consistent with the recent studies incorporating data from *Gaia* DR2 (e.g. Hattori et al. 2018, Monari et al. in preparation). In turn this implies a higher total mass for the Milky Way in agreement with recent analyses of the orbits of globular clusters using *Gaia* DR2 astrometric data (e.g. Watkins et al. 2018; Posti & Helmi 2018). We note that these higher total (dark matter) masses imply increased dark matter substructure and higher numbers of satellite galaxies (Fattahi et al. 2016), with obvious ramifications for the ‘missing satellite’ issue (e.g. Bullock & Boylan-Kolchin 2017)

The identification of HVS is both timely, given the release of the exquisite *Gaia* astrometric data, and necessary, given our understanding of the supermassive black hole and surrounding stellar population in the Galactic centre region. The discovery of many stars with extreme kinematics will ultimately allow us to understand the parent population of HVS to constrain the production mechanism(s) that dominates their creation. The results presented here demonstrate

the power of combining *complementary* approaches of dynamical orbit integration analysis and chemical characterisation to constrain the origins of HVSs and ultimately to provide a better understanding of these rare stars and the physical mechanisms that produce them.

APPENDIX A: ONLINE TABLES

We provide an online table, a section of which is shown in Table A1 for reference. This table includes the line-by-line abundances for each star, line and elemental species. The table also includes the atomic data, specifically the oscillator strength ($\log gf$), the wavelength (Å), and excitation potential (in eV) for each line.

ACKNOWLEDGEMENTS

We thank the referee for their detailed and constructive comments that improved this manuscript. K.H. would like to thank Kohei Hattori, Nathan Leigh, Marwan Gerbran, Douglas Boubert, James Guillochon, and Idan Ginsburg for lively discussions. RFGW thanks her sister, Katherine Barber, for her support. RFGW also thanks the Leverhulme Trust for a Visiting Professorship at the University of Edinburgh, held while this work was being completed. We would also like to thank Scott Kenyon for his detailed comments. Based on observations obtained with the Apache Point Observatory 3.5-meter telescope, which is owned and operated by the Astrophysical Research Consortium. We thank all at APO for their assistance during remote observing. This project was developed in part at the 2018 NYC Gaia Sprint, hosted by the Center for Computational Astrophysics of the Flatiron Institute in New York City.

This work has made use of data from the European Space Agency (ESA) mission *Gaia* (<https://www.cosmos.esa.int/gaia>), processed by the *Gaia* Data Processing and Analysis Consortium (DPAC, <https://www.cosmos.esa.int/web/gaia/dpac/consortium>). Funding for the DPAC has been provided by national institutions, in particular the institutions participating in the *Gaia* Multilateral Agreement.

REFERENCES

- Abadi M. G., Navarro J. F., Steinmetz M., 2009, *ApJ*, **691**, L63
 Alvarez R., Plez B., 1998, *A&A*, **330**, 1109
 Andrae R., et al., 2018, preprint, ([arXiv:1804.09374](https://arxiv.org/abs/1804.09374))
 Andrievsky S., Bonifacio P., Caffau E., Korotin S., Spite M., Spite F., Sbordone L., Zhukova A. V., 2018, *MNRAS*, **473**, 3377
 Asplund M., Grevesse N., Sauval A. J., 2005, in Barnes III T. G., Bash F. N., eds, *Astronomical Society of the Pacific Conference Series Vol. 336, Cosmic Abundances as Records of Stellar Evolution and Nucleosynthesis*. p. 25
 Astraatmadja T. L., Bailer-Jones C. A. L., 2016, *ApJ*, **832**, 137
 Bastian N., Lardo C., 2017, preprint, ([arXiv:1712.01286](https://arxiv.org/abs/1712.01286))
 Battistini C., Bensby T., 2015, *A&A*, **577**, A9
 Battistini C., Bensby T., 2016, *A&A*, **586**, A49
 Beers T. C., Drilling J. S., Rossi S., Chiba M., Rhee J., Fuhrmeister B., Norris J. E., von Hippel T., 2002, *AJ*, **124**, 931
 Bensby T., Feltzing S., Oey M. S., 2014, *A&A*, **562**, A71
 Blaauw A., 1961, *Bull. Astron. Inst. Netherlands*, **15**, 265
 Boubert D., Evans N. W., 2016, *ApJ*, **825**, L6
 Boubert D., Erkal D., Evans N. W., Izzard R. G., 2017, *MNRAS*, **469**, 2151
 Boubert D., Guillochon J., Hawkins K., Ginsburg I., Evans N. W., 2018, preprint, ([arXiv:1804.10179](https://arxiv.org/abs/1804.10179))
 Bromley B. C., Kenyon S. J., Geller M. J., Barcikowski E., Brown W. R., Kurtz M. J., 2006, *ApJ*, **653**, 1194
 Bromley B. C., Kenyon S. J., Brown W. R., Geller M. J., 2009, *ApJ*, **706**, 925
 Brown W. R., 2015, *ARA&A*, **53**, 15
 Brown W. R., Geller M. J., Kenyon S. J., Kurtz M. J., 2005, *ApJ*, **622**, L33
 Brown W. R., Lattanzi M. G., Kenyon S. J., Geller M. J., 2018, preprint, ([arXiv:1805.04184](https://arxiv.org/abs/1805.04184))
 Buder S., et al., 2018, preprint, ([arXiv:1804.06041](https://arxiv.org/abs/1804.06041))
 Bullock J. S., Boylan-Kolchin M., 2017, *ARA&A*, **55**, 343
 Carney B. W., Latham D. W., Laird J. B., Aguilar L. A., 1994, *AJ*, **107**, 2240
 Chiba M., Beers T. C., 2000, *AJ*, **119**, 2843
 Edelman H., Napiwotzki R., Heber U., Christlieb N., Reimers D., 2005, *ApJ*, **634**, L181
 Eggen O. J., Lynden-Bell D., Sandage A. R., 1962, *ApJ*, **136**, 748
 Erkal D., Boubert D., Gualandris A., Evans N. W., Antonini F., 2018, preprint, ([arXiv:1804.10197](https://arxiv.org/abs/1804.10197))
 Fattahi A., et al., 2016, *MNRAS*, **457**, 844
 Frebel A., Casey A. R., Jacobson H. R., Yu Q., 2013, *ApJ*, **769**, 57
 Gaia Collaboration Brown A. G. A., Vallenari A., Prusti T., de Bruijne J. H. J., Babusiaux C., Bailer-Jones C. A. L., 2018, preprint, ([arXiv:1804.09365](https://arxiv.org/abs/1804.09365))
 Gilmore G., Wyse R. F. G., 1998, *AJ*, **116**, 748
 Gualandris A., Portegies Zwart S., 2007, *MNRAS*, **376**, L29
 Gustafsson B., Edvardsson B., Eriksson K., Jørgensen U. G., Nordlund Å., Plez B., 2008, *A&A*, **486**, 951
 Hattori K., Valluri M., Bell E. F., Roederer I. U., 2018, preprint, ([arXiv:1805.03194](https://arxiv.org/abs/1805.03194))
 Hawkins K., et al., 2015, *MNRAS*, **447**, 2046
 Hawkins K., et al., 2016, *A&A*, **592**, A70
 Hills J. G., 1988, *Nature*, **331**, 687
 Iwamoto K., Brachwitz F., Nomoto K., Kishimoto N., Umeda H., Hix W. R., Thielemann F.-K., 1999, *ApJS*, **125**, 439
 Jofré P., et al., 2014, *A&A*, **564**, A133, Paper III
 Kenyon S. J., Bromley B. C., Geller M. J., Brown W. R., 2008, *ApJ*, **680**, 312
 Kobayashi C., Nakasato N., 2011, *ApJ*, **729**, 16
 Kobayashi C., Umeda H., Nomoto K., Tominaga N., Ohkubo T., 2006, *ApJ*, **653**, 1145
 Kunder A., et al., 2017, *AJ*, **153**, 75
 Luo A.-L., et al., 2015, *Research in Astronomy and Astrophysics*, **15**, 1095
 Majewski S. R., et al., 2017, *AJ*, **154**, 94
 Marchetti T., Rossi E. M., Brown A. G. A., 2018, preprint, ([arXiv:1804.10607](https://arxiv.org/abs/1804.10607))
 Masseron T., et al., 2014, *A&A*, **571**, A47
 Masseron T., Merle T., Hawkins K., 2016, BACCHUS: Brussels Automatic Code for Characterizing High accuracy Spectra, Astrophysics Source Code Library (ascl:1605.004), [doi:10.20356/C4TG6R](https://doi.org/10.20356/C4TG6R)
 Matteucci F., Recchi S., 2001, *ApJ*, **558**, 351
 McWilliam A., 2016, *Publ. Astron. Soc. Australia*, **33**, e040
 Mishenina T. V., Kovtyukh V. V., Soubiran C., Travaglio C., Busso M., 2002, *A&A*, **396**, 189
 Nomoto K., Kobayashi C., Tominaga N., 2013, *ARA&A*, **51**, 457
 Piffl T., et al., 2014, *A&A*, **562**, A91
 Plez B., 2012, Turbospectrum: Code for spectral synthesis, Astrophysics Source Code Library (ascl:1205.004)
 Posti L., Helmi A., 2018, preprint, ([arXiv:1805.01408](https://arxiv.org/abs/1805.01408))
 Poveda A., Ruiz J., Allen C., 1967, *Boletín de los Observatorios Tonantzintla y Tacubaya*, **4**, 86
 Roederer I. U., Preston G. W., Thompson I. B., Shtetman S. A., Sneden C., Burley G. S., Kelson D. D., 2014, *AJ*, **147**, 136
 Rossi E. M., Marchetti T., Cacciato M., Kuiack M., Sari R., 2017, *MNRAS*, **467**, 1844

Table A1. Line-By-Line Chemical Abundances and Atomic Information

Star	Element	λ (\AA)	$\log(gf)$	Excitation Pot. (eV)	$\log(\epsilon)$
1508756353921427328	Ca I	5260.38	-1.719	2.521	4.949
1508756353921427328	Ca I	5261.70	-0.579	2.521	4.678
1508756353921427328	Ca I	5349.46	-0.310	2.709	4.863
1508756353921427328	Ca I	5512.98	-0.464	2.933	4.900
1508756353921427328	Ca I	5581.96	-0.555	2.523	4.766
1508756353921427328	Ca I	5588.74	0.358	2.526	4.311
1508756353921427328	Na I	5682.63	-0.706	2.102	4.091
1508756353921427328	Na I	5688.20	-0.404	2.104	4.462
1508756353921427328	Na I	6160.74	-1.246	2.104	4.375
1508756353921427328	Na I	8183.25	0.237	2.102	4.547
1364548016594914560	Na I	4497.65	-1.574	2.104	5.068
1364548016594914560	Na I	5682.63	-0.706	2.102	4.827
1364548016594914560	Na I	5688.20	-0.404	2.104	4.881
1364548016594914560	Na I	6160.74	-1.246	2.104	4.784
...

The *Gaia* DR2 source id is tabulated in column 1. The element, wavelength (\AA), oscillator strength ($\log(gf)$), and excitation potential (in eV) for each absorption feature consider in each star is in column 2, 3, 4, and five, respectively. The last column of the table indicates the derived abundance for each absorption feature in each star.

- Ruchti G. R., et al., 2011, *ApJ*, **737**, 9
Samland M., 1998, *ApJ*, **496**, 155
Shen K. J., et al., 2018, preprint, ([arXiv:1804.11163](https://arxiv.org/abs/1804.11163))
Silk J., Antonuccio-Delogu V., Dubois Y., Gaibler V., Haas M. R.,
Khochar S., Krause M., 2012, *A&A*, **545**, L11
Smith M. C., et al., 2007, *MNRAS*, **379**, 755
Steinmetz M., et al., 2006, *AJ*, **132**, 1645
Van der Swaelmen M., Hill V., Primas F., Cole A. A., 2013, *A&A*,
560, A44
Wang X., Loeb A., 2017, preprint, ([arXiv:1706.04201](https://arxiv.org/abs/1706.04201))
Watkins L. L., van der Marel R. P., Sohn S. T., Evans N. W.,
2018, preprint, ([arXiv:1804.11348](https://arxiv.org/abs/1804.11348))
Williams A. A., Belokurov V., Casey A. R., Evans N. W., 2017,
MNRAS, **468**, 2359
Xiang M.-S., et al., 2017, *MNRAS*, **467**, 1890
Yong D., et al., 2013, *ApJ*, **762**, 26
Yu Q., Tremaine S., 2003, *ApJ*, **599**, 1129

This paper has been typeset from a $\text{\TeX}/\text{\LaTeX}$ file prepared by the author.